Design of Thin-Walled Steel Structures Susceptible to Interactive Buckling

CIVE70009 - Civil Engineering Individual Research Project 2024-2025

Department of Civil and Environmental Engineering Imperial College London

Ersid Alushi (CID: 06032773)

Supervisor:
Prof. Ahmer Wadee
Dr. Xin Meng
Prof. Francesco Tondolo

Abstract

This final year's project investigates the interactive buckling behavior of thin-walled rectangular steel section columns subjected to axial compression through a point load. These structural members can be efficient and lightweight but can also be highly sensitive during the interaction of local ang global buckling phenomena. This interaction might result in instability which leads to premature failure and imperfection sensitivity, posing challenges to the current design approaches. Finite element analysis (FEA) has been used by ABAQUS software to precisely simulate the realistic effects of the boundary conditions, material nonlinearity, geometric imperfections and residual stresses. Particular attention was given to the presence of residual stress due to the welding process, since they have shown a significant reduction in structural capacity. The validation process involved comparison against experimental data from Yang et al. (2017) and numerical studies by Shen & Wadee (2019a), demonstrating good agreement in failure modes and ultimate load predictions. Proceeding with an automated GMNIA (Geometrically and Materially Nonlinear Imperfect Analysis) using a Python script, this project conducted extensive parametric studies efficiently. The extracted data was then compared with Eurocode 3 (EC3) design curves, showing conservative and non-conservative discrepancies. To address the present limitations of the Effective Width Method (EWM), a new normalization approach was adopted. The findings demonstrate the need for an improvement of design guidance and the importance of including both interaction effects and residual stresses during the stability assessment.

Index

1. Introduction	
2. Literature review	2
2.1 Local and global interactive buckling	2
2.2 Finite element modelling of thin-walled box section column	2
2.3 Overview of current design for thin-walled steel columns	3
3. Finite element framework and validation	4
3.1 Geometry and boundary conditions	4
3.2 Material modelling	4
3.3 Geometric imperfections	6
3.4 Residual Stresses	6
3.5 Model Validation	7
3.5.1 Experimental results from Yang et al. (2017)	8
3.5.2 FE results from Shen & Wadee (2019a)	14
3.6 Automatization of the GMNIA	16
3.6.1 Automatization overview	16
3.5.1 Automated GMNIA's algorithm	17
4. Design standards and preliminary analysis	18
4.1 EC3 design guidance	18
4.1.1 Flexural buckling design in EC3 (2005)	18
4.1.2 Local buckling design in EC3 (2006)	19
4.1.3 Interaction between global and local buckling in EC3 (2005)	20
4.2 FE model and EC3 design curve comparison	21
5. Parametric study	24
5.1 Global slenderness using A _{eff}	24
5.1.1 Reduction factor vs Global slenderness	24
5.1.2 Critical loads ratio vs Ultimate loads ratio	26
5.2 Global slenderness using gross area A	28
5.2.1 Reduction factor vs Global slenderness	28
5.2.2 Critical loads ratio vs Ultimate loads ratio	29
6. Conclusions	30
7. Acknowledgments	31
8 References	32

1. Introduction

Civil engineering continues to advance bringing to an expansion of structural design considerations beyond fundamental factors such as safety, strength and stiffness. Additional focus has been turned on aspects such as long-term performance, material efficiency and environmental sustainability. The involvement of thin-walled components plays a crucial role in dealing with sustainability, becoming widely used in structural components, particularly in steel structures.

Thin-walled components generally have a relatively small wall thickness relative to their overall size, such as length and width. These structural elements are designed to carry efficiently the loads while minimizing the amount of the material used. Furthermore, when multiple thin-walled elements are transformed into composite structures, they often demonstrate a stable behavior even after buckling occurs, enhancing further the strength and cost of the component.

This type of steel has been adopted in high-rise buildings, bridge decks, offshore platforms and lightweight industrial warehouses primarily due to their high strength-to-weight ratio or ease to assemble. Facing the nowadays sustainability problems, the thin-walled steel elements become very efficient in reducing the incorporated carbon within the structural environment.

Understanding the buckling behaviour is not important just for theoretical modeling but it has also direct implications for safe and economical design. Offshore wind turbine tower, long span bridges or tall transmission mast are widely composed by thin-walled elements where local-global buckling interaction can interfere with design safety margins. In these cases, being too conservative may lead to unnecessary material use and bigger costs. On the other hand, unconservative predictions can result in unsafe structures.

Even though thin-walled components bring many advantages, they can be susceptible to local buckling phenomena. The occurrence of buckling can be acceptable since it shows full utilization of material strength and stiffness. However, global buckling can be present under compressive loads if the slenderness is considerable. Both bucking modes have different critical loads and their interaction can be analyzed by comparing the critical values. When these two buckling modes have a simultaneous occurrence, they can lead to an instability from post-buckling behavior and significant imperfection sensitivity (Bai & Wadee, 2015).

During manufacturing and construction, factors like geometric imperfections and residual stresses may arise. These factors can have a direct impact on the buckling response of the component (Behzadi et al.2021).

During many years a substantial amount of research has been conducted on buckling analyses and still the design codes continue to treat local and global buckling separately without considering their interaction following the coupled failure modes. This brings to a very conservative design that fails to fully use material strength.

The aim of this final year project is to integrate the advanced analytical models, finite element simulations and experimental data to have a better understanding of the interactive buckling of

thin-walled box section structures. This way we have a better connection between theoretical studies and real-world applications.

2. Literature review

2.1 Local and global interactive buckling

Understanding the stability of structural elements under compressive loads is critical for evaluating their ultimate strength. With time engineers have gained deeper awareness of this phenomenon through extensive research. Buckling normally occurs when the structural elements involved have a high slenderness ratio and this can be the case of the thin-walled structures (Rozylo, Rogala & Pasnik 2023). The buckling behavior can be classified into two categories: global and local. When these modes occur separately, the post-buckling behavior can be neutral or weakly stable. But when we have a present interaction, it brings an unpredictable and hazardous behavior.

Furthermore, interactive buckling is highly sensitive to factors that can affect the structural response such as geometric imperfections, residual stresses and material nonlinearity. Numerical experimental studies (Degée, Detzel & Kuhlmann 2008) have suggested that in thin-walled structures under compression the failure does not come as a result of buckling itself, but from reaching the material's ultimate stress.

Early research about the interactive buckling saw a major improvement with Van der Neut's work, demonstrating that local and global buckling are not independent phenomena, but they can influence each other (Van der Neut, 1969). Developing Koiter's theory (W.T. Koiter, 1945), Van der Neut simplified the theoretical considering two load-carrying flanges and rigid webs with no longitudinal stiffness. The webs functioned as constraints, working as simply supported boundary conditions to the flanges. This model would help investigate the initial post-buckling response and imperfection sensitivity, identifying the results of the interactive buckling in columns. Although the model offered valuable early insights, it did not fully capture the complexity of interactions between plates within the full cross-section.

2.2 Finite element modelling of thin-walled box section column

Computer technology advancing every day, finite element analysis (FEA) has become a great method for studying the buckling behavior of structural members and allowing the application of the actual stress distribution. This approach has been widely used due to its efficiency, flexibility and ability to perform complex structural analysis. ABAQUS is a particular software for the FE providing a comprehensive modelling environment, advanced tools and editing options through scripting.

Since finite element (FE) modelling allows us to add an accurate representation of material behavior, researchers have developed various models to achieve this. One of them is the bilinear

plus nonlinear hardening model where with precision it captures all the material strain-hardening effects (Yun & Gardner, 2017).

Another critical challenge in numerical modelling is introducing the initial geometric imperfections, since there are no perfect geometries in real life structures. Accounting that their identification cannot be established easily, a linear buckling analysis is required to identify the particular buckling modes to create the basis for the imperfection's application. Normally the lowest order buckling mode would play a major role in the structural response definition (Meng & Gardner 2021).

Degée, Detzel & Kuhlmann (2008) have shown that the interaction between residual stresses and geometric imperfections can have a great impact on the buckling phenomenon. This way they proposed an equivalent imperfection approach to take into account the effects in a finite element analysis. Pavlović et al. (2012) later demonstrated that this methodology was overly optimistic and that it required additional refinement. They suggested that in the presence of both residual stresses and imperfections, the maximum local imperfections need to be limited to 1/1000 of the section's height ensuring a more reliable and safe structural design.

2.3 Overview of current design for thin-walled steel columns

According to EN 1993-1-1 (2005) and EN 1993-1-5 (2006), the design provision often relies on the Effective Width Method (EWM) since it is the most common approach used to assess members like thin-walled steel columns affected by both local and global interactions. This method takes into account both instability modes simultaneously by introducing the global buckling reduction factor χ and the effective cross-sectional area $A_{\rm eff}$.

This direct multiplication, that often has a conservative result, has brought researchers to prove that is not always the case. Experimental compression tests on thin-walled steel columns with various geometries have shown that Eurocode 3 (EC3) predictions were unconservative, giving an underestimation of the actual structural response (Yang et al. 2017). This emphasizes the need for more refinement in existing design rules regarding interactive buckling.

Meng & Gardner (2020) through analysis of thin-walled steel columns with different material strengths noticed differences between the EC3 predictions and experimental results. In order to demonstrate improved accuracy, particularly in cold-formed steel, they proposed several modifications to EC3's interactive buckling equations.

In addition to the Effective Width Method, the Direct Strength Path (DSM) was initially developed for the design of cold-formed steel. However, Kwon & Seo (2013) later introduced a modified DSM formula to be extended also for welded rectangular sections based on experimental and numerical results.

Building on these findings, Shen and Wadee (2019b) created finite element simulations and reliability assessments. Their work concluded that for welded rectangular thin-walled columns under interactive buckling, the modified DSM provided more reliable predictions than both the standard DSM and EWM formulations from EC3.

3. Finite element framework and validation

In this final year project, the ABAQUS engineering simulation software will be used to build finite element models to compare with the experimental data. Since our interest is focused on buckling interaction phenomena, thin-walled box-section columns will be considered under a purely axial load *P*. Shell elements will be used for simplified modelling, since section thickness affects buckling behavior. On the next steps of the process, we will discuss the implementation on model of boundary conditions, material nonlinearity, geometric imperfections and residual stresses.

3.1 Geometry and boundary conditions

The project's focus is on investigating the interactive buckling response of thin-walled rectangular section columns subjected to compression with residual stresses present as well. The geometric visualization of the column is provided below, where B and H represent the width and height of the section and wall thickness t for all sides, while the column length is denoted as L. The ends of the columns are supported using pin-end connections to replicate the support conditions.

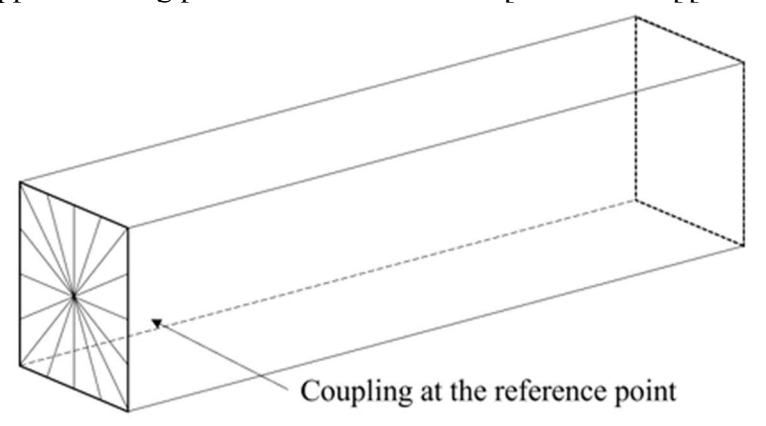


Figure 1 Illustration of the FE model rigid body coupling

To ensure proper load transfer in the finite element model, nodes located at the ends of the member are linked to reference points placed at the centroids of the respective end cross-sections. This can be implemented by the rigid body kinematic coupling in ABAQUS allowing the distribution of the axial load in each node. These reference points are set up to restrict translations and rotations where necessary, by satisfying the pin-end boundary conditions while allowing appropriate degrees of freedom of each end-section.

Given the influence of geometric and material nonlinearity in buckling behavior, a nonlinear analysis is required. Accordingly, the Riks arc-length method is adopted to trace the full equilibrium path and capture the instability phenomena throughout the analysis.

3.2 Material modelling

During this project, the material is considered to be isotropic and homogeneous, including strain hardening behavior. The fundamental material properties are selected to match the ones used in

the experimental tests, such as Young's modulus E, Poisson's ratio ν and shear modulus $G=E/[2(1+\nu)]$.

To make the direct comparison easier between experimental results and finite element (FE) simulations, multiple FE models will be constructed under identical conditions, with the only change in their constitutive relationships. The bi-linear plus nonlinear hardening model represents the qualitative description of the constitutive relationship of the model, but the idealized piecewise linear hardening model will be used to simulate the actual relationship. The stress-strain relationship curves are shown in the figure below. The key parameters include the yielding stress f_y , the ultimate stress f_u , the yielding strain ε_y , the ultimate strain ε_u and the strain ε_{st} representing the value beyond which the strain hardening begins.

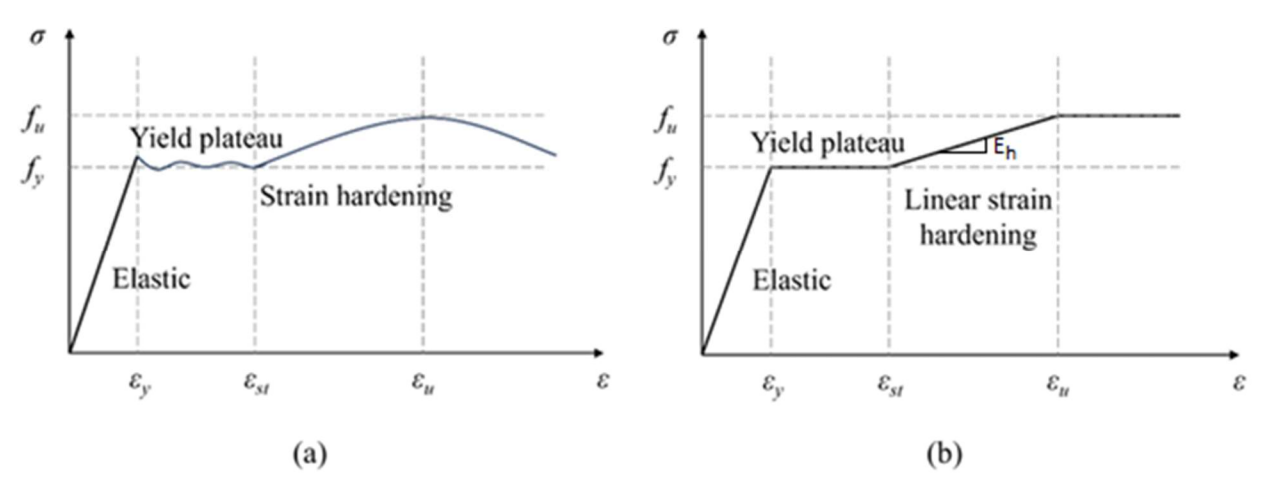


Figure 2 (a) bi-linear plus nonlinear hardening model (qualitative description); (b) idealized piecewise linear hardening model

It is necessary to be noted that ε_{st} is given by $(1+n)\varepsilon_y$ and E_h is the slope of the strain-hardening process referred to as the effective Young's modulus. The following equation (Yun & Gardner, 2017) describes the bi-linear plus nonlinear elastic-plastic constitutive relationship:

$$f(\varepsilon) = \begin{cases} \varepsilon & \text{for } \varepsilon \leq \varepsilon_{y} \\ f_{y} & \text{for } \varepsilon_{y} < \varepsilon \leq \varepsilon_{st} \end{cases}$$

$$f(\varepsilon) = \begin{cases} f_{y} + (f_{u} + f_{y}) \left\{ 0.4 \left(\frac{\varepsilon - \varepsilon_{st}}{\varepsilon_{u} - \varepsilon_{st}} \right) + \frac{2 \left(\frac{\varepsilon - \varepsilon_{st}}{\varepsilon_{u} - \varepsilon_{st}} \right)^{\frac{1}{5}}}{\left[1 + 40 \left(\frac{\varepsilon - \varepsilon_{st}}{\varepsilon_{u} - \varepsilon_{st}} \right)^{5} \right]^{\frac{1}{5}}} \end{cases}$$

$$for \varepsilon_{st} < \varepsilon \leq \varepsilon_{u}$$

$$(3.1)$$

The constitutive relationships presented in Fig.2 are taken as nominal values for stress and strain without considering the reduction of the cross-sectional area during loading. Since in ABAQUS the constitutive formulation is based on the true Cauchy constitutive relationship, it is required to transform the engineering values of stress and strain into true stress and strain.

$$\sigma_{true} = \sigma_{engineering} (1 + \varepsilon_{engineering}) \tag{3.2}$$

$$\varepsilon_{true} = ln(1 + \varepsilon_{engineering})$$
(3.3)

$$\varepsilon_{pl,true} = \varepsilon_{true} - \frac{\sigma_{true}}{E} \tag{3.4}$$

3.3 Geometric imperfections

In this part, geometric imperfections are incorporated in the model to better capture both local and global imperfections, ensuring that the representation of buckling interaction is accurate. Local imperfections are assumed to follow a sinusoidal distribution being the lowest local buckling mode of the component. Meanwhile, the global imperfections are represented by a half-sine wave distribution. The distribution patterns of these imperfections are illustrated below.

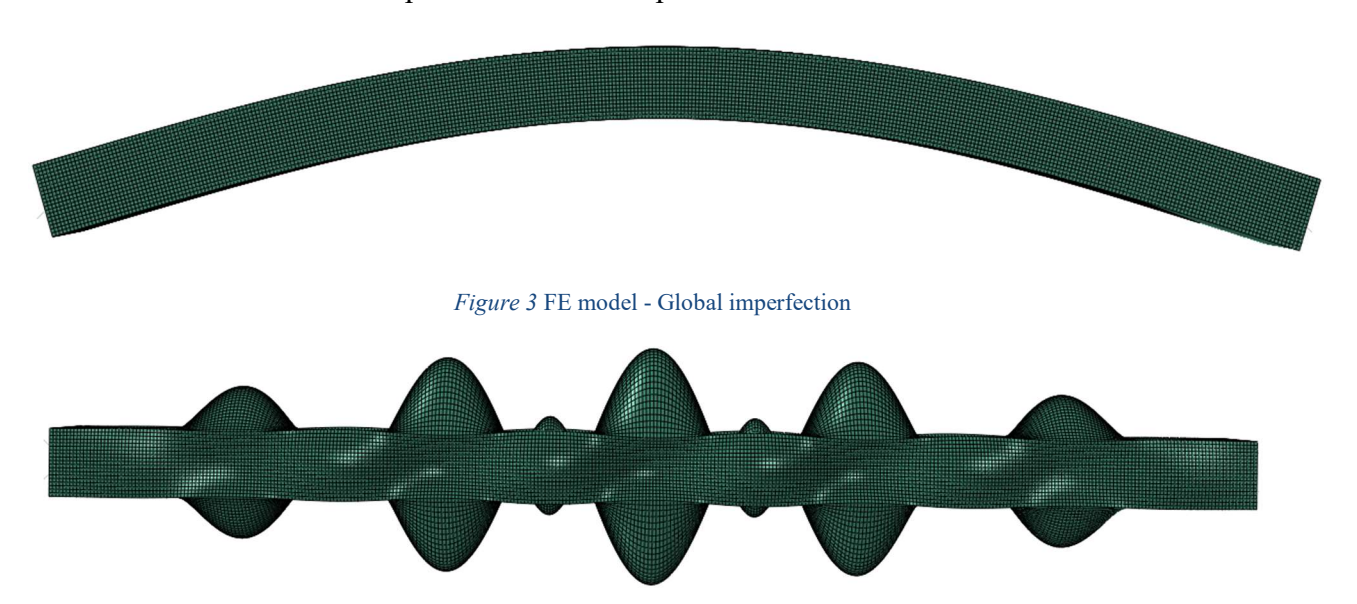


Figure 4 FE model - Local imperfection

Once the shapes of the imperfections are established, it is necessary to define properly their amplitudes. As stated in Eurocode 3 (EC3), the recommended maximum amplitude for global imperfections corresponds to the member length divided by 1000, while for local buckling imperfections we take the section width divided by 200. With the combination of the necessary adjustments of the geometric imperfections now with the residual stresses, the FE model becomes more similar to the experimental tests.

In ABAQUS, the geometric imperfections are introduced using the "*imperfection" command. The process begins with a linear buckling analysis to extract the local and global buckling modes and storing the relative displacements of the nodes. Editing the keyword of the model we are finally able to import the node file containing the displacements and use it as the geometric imperfection.

3.4 Residual Stresses

Numerous researches have been conducted on residual stress and there have been different model proposals. Nevertheless, many of these models are designed for certain welding procedures or

materials, which brings to a limiting application for our project. Consequently, we will be adopting the residual stress distribution model from the European Convention for Constructional Steelwork (ECCS) for welded rectangular hollow section members.

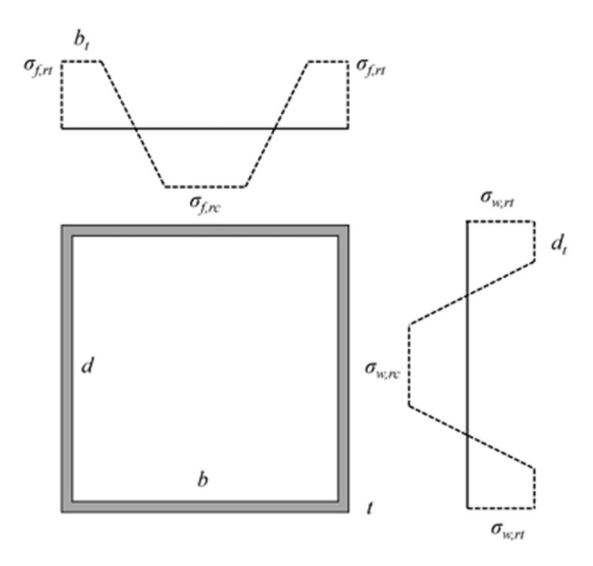


Figure 5 ECCS's residual stress distribution model

According to this model, the regions near the weld go through tensile residual stress $\sigma_{w,rt}$, set at the material's yield strength f_y . Meanwhile, regions located further from the weld are subjected to compressive residual stress $\sigma_{w,rc}$, and it can be calculated with the following relationship:

$$\sigma_{w,rc} = \frac{3d_t \sigma_{w,rt}}{d - 3d_t} \tag{3.5}$$

where d_t denotes the width of the part under tensile stress and its value can vary depending on the welding procedure. For lightly-welded section, d_t is taken as 1.5 times the section thickness, whereas for heavily-welded sections, d_t is taken as three times the section thickness.

In the FE models residual stress will be modeled as initial membrane stress. This requires an equilibrium state check to ensure that the residual stress has been applied in the correct way. According to Shen & Wadee (2019a), when we have simultaneously applied residual stress and geometric imperfections, it can create an effect that leads to an amplification of the imperfection. This brings to a careful consideration as it can have a great effect on the structural behavior and stability.

3.5 Model Validation

To validate the accuracy of the column modelling process with its appropriate parameters, a comparison is held between ultimate load values and the general trend of the force-displacement curve with both experimental results from Yang et al. (2017) and the finite element model results from Shen & Wadee (2019a).

3.5.1 Experimental results from Yang et al. (2017)

The test specimens used from Yang's paper are summarized in the following tables indicating the geometric and material properties. By applying these properties to the model as described in the previous chapters, it is possible to derive the force-displacement curve.

Table 1 Geometric properties of the specimens (Yang et al., 2017)

Specimen	B /mm	D/mm	t/mm	L_{e}/mm
R-235-1	135,5	254,1	5,48	2251,6
R-235-2	160,7	310,8	5,45	2780,4
R-235-3	158	309	5,59	4159,9
R-235-4	210	404,5	5,44	3585,3
R-235-5	251,4	491,2	5,44	4378,1
R-345-1	131,2	251,7	5,81	2255
R-345-2	161,8	312,5	5,69	2786,9
R-345-3	163	312,1	6,05	4165,6
R-345-4	209,5	403,4	5,82	3582,4
R-345-5	251	491,7	5,8	4375,6

Table 2 Material properties of the specimens (Yang et al., 2017)

Specimen	E/MPa	f_y / MPa	$\mathcal{E}_{\mathcal{Y}}$	\mathcal{E}_{st}	f_u/MPa	\mathcal{E}_{u}
T-235-1	2,07E+05	286,45	0,00138	0,0312	432,2	0,167
T-235-2	2,11E+05	290,89	0,00138	0,0243	441,51	0,179
T-235-3	2,09E+05	311,78	0,00149	0,0316	468,32	0,18
T-235-4	2,08E+05	321,81	0,00155	0,0234	464,54	0,186
T-235-5	2,10E+05	328,36	0,00156	0,0207	483,69	0,184
T-235-6	2,07E+05	315,3	0,00152	0,0265	462,48	0,21
T-235-7	2,05E+05	310,4	0,00151	0,0284	454,91	0,189
T-345-1	1,95E+05	351,62	0,0018	0,0153	514,81	0,184
<i>T-345-2</i>	1,97E+05	383,85	0,00195	0,0168	546,26	0,166
<i>T-345-3</i>	2,03E+05	416,25	0,00205	0,0145	575,91	0,132
T-345-4	1,91E+05	376,98	0,00198	0,0109	535,59	0,131
T-345-5	2,01E+05	397,59	0,00198	0,0148	556	0,129

As for the initial geometric imperfections, measurements like the maximum out-of-straightness deformation at mid-span and maximum displacement of the four plates were saved to be used in the next steps as the local and global imperfections in the FE model. Meanwhile, for the residual stress, the actual distribution was not provided, meaning that the ECCS distribution model was used. It has been assumed that the specimens were heavily welded, which brings the parameter d_t to considered as three times the section thickness.

With all the parameters established in the FE model, the final failure mode was obtained. This provided another comparison with the actual experimental behavior. As shown below, the failure mode of the FE model is very similar to the one from the experiments.



Figure 6 FE model and experiment comparison of failure mode



Figure 7 Failure mode in detail

The relationship between the displacement of the column and the axial force during the real experiment can be validated against the data obtained from the Finite Element model. Different displacement directions were considered in order to have a clearer understanding. The model under consideration for this particular comparison is going to be R-235-2.

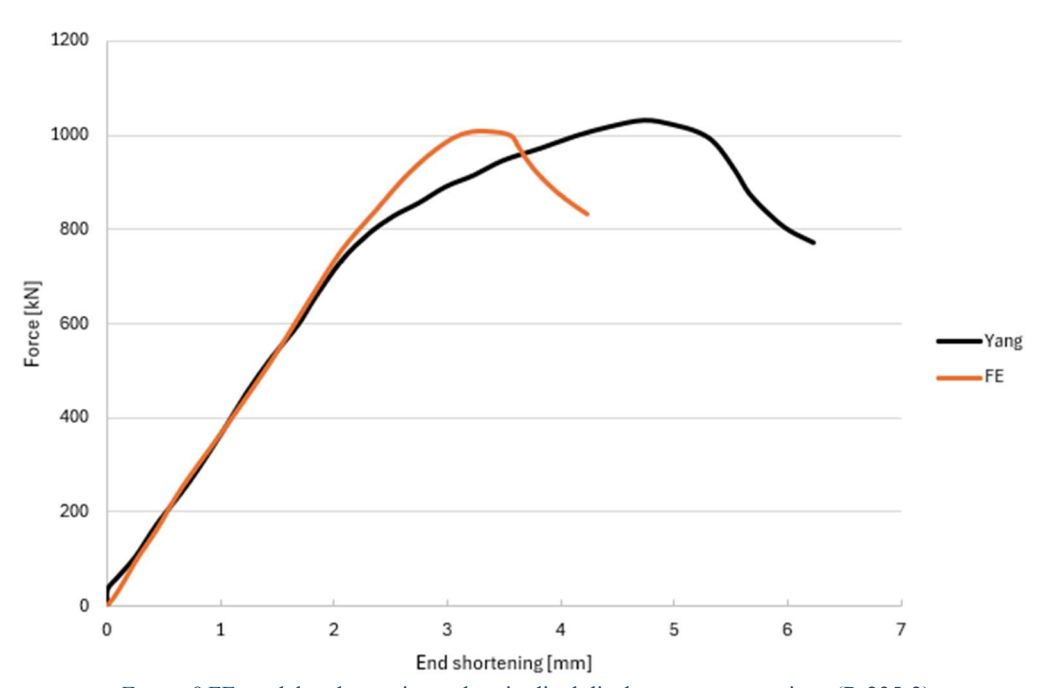


Figure 8 FE model and experiment longitudinal displacement comparison (R-235-2)

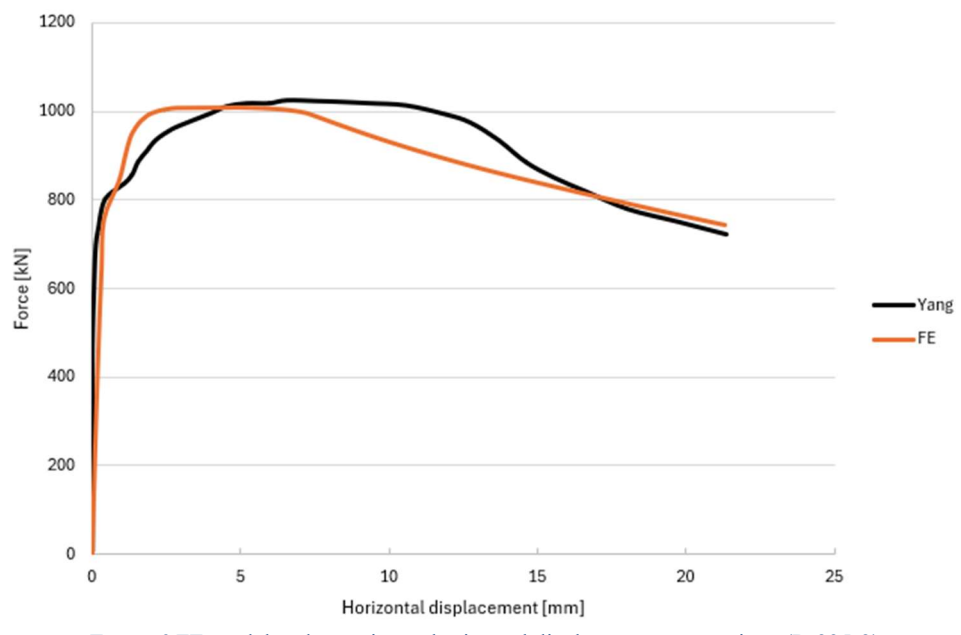


Figure 9 FE model and experiment horizontal displacement comparison (R-235-2)

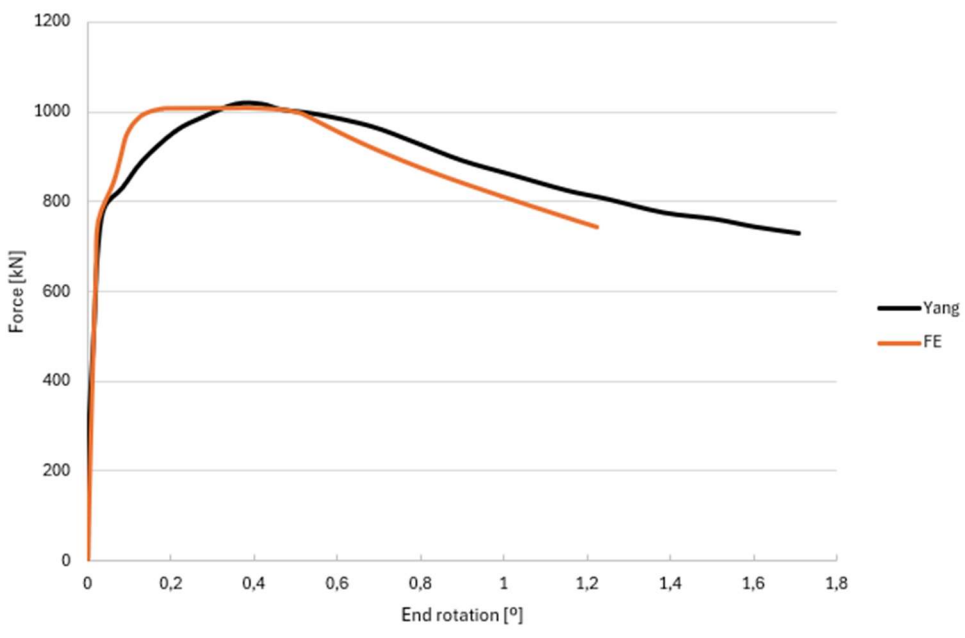


Figure 10 FE model and experiment end rotation comparison (R-235-2)

As it can be noticed, the value of the ultimate load obtained from the FE model remains within the acceptable error range when compared to the one obtained from the experiments held from Yang et al. (2017). Regarding the difference along the displacement for all three figures from above, it can be said, as expected, the real life displacement behavior of an experimental sample cannot be alike from the one obtained from a finite element model.

To fully understand the behavior of rectangular hollow section (RHS) columns under axial load, it is necessary to perform multiple comparisons: the full model including geometric imperfections and residual stresses (case 1), the model without residual stresses (case 2), the model without local

imperfections (case 3) and the model without global imperfections (case 4). Finally, for each case, it is compared to the ultimate load captured by the FE model with the experimental result.

Table 3 Ultimate load experiment and FE model (case 1)

ALL

Specimen	Pult, exp / kN	Pult, FE / kN	FE/Exp	Mean	SD	COV
R-235-1	1057,7	928,48	0,88			
R-235-2	1029,1	1009,77	0,98			
R-235-3	1176,9	1068,70	0,91			
R-235-4	1284,6	1216,30	0,95			
R-235-5	1287,6	1301,81	1,01	0.07	0.05	0.05
R-345-1	1164,4	1139,06	0,98	0,97	0,05	0,05
R-345-2	1414,6	1378,39	0,97			
R-345-3	1172,8	1129,90	0,96			
R-345-4	1456,7	1500,91	1,03			
R-345-5	1431,1	1503,80	1,05			

Table 4 Ultimate load experiment and FE model (case 2)

No Residual Stress

Specimen	Pult, exp / kN	Pult, FE / kN	FE/Exp	Mean	SD	COV
R-235-1	1057,7	1043,88	0,99			
R-235-2	1029,1	1214,94	1,18			
R-235-3	1176,9	1190,99	1,01			
R-235-4	1284,6	1375,39	1,07			
R-235-5	1287,6	1431,64	1,11	1 12	0.00	0.00
R-345-1	1164,4	1480,31	1,27	1,13	0,09	0,08
R-345-2	1414,6	1534,56	1,08			
R-345-3	1172,8	1397,00	1,19			
R-345-4	1456,7	1703,26	1,17			
R-345-5	1431,1	1767,29	1,23			

Table 5 Ultimate load experiment and FE model (case 3)

No Local Imperfections

Specimen	Pult, exp / kN	Pult, FE / kN	FE/Paper	Mean	SD	COV
R-235-1	1057,7	965,74	0,91			
R-235-2	1029,1	1180,18	1,15			
R-235-3	1176,9	1246,96	1,06			
R-235-4	1284,6	1442,92	1,12			
R-235-5	1287,6	1479,73	1,15	1 11	0,10	0.00
R-345-1	1164,4	1453,82	1,25	1,14	0,10	0,09
R-345-2	1414,6	1544,92	1,09			
R-345-3	1172,8	1430,25	1,22			
R-345-4	1456,7	1682,03	1,15			
R-345-5	1431,1	1785,31	1,25			

Table 6 Ultimate load experiment and FE model (case 4)

No Global Imperfections

		1 3					
Specimen	Pult, exp / kN	Pult, FE / kN	FE/Paper	Mean	SD	COV	
R-235-1	1057,7	915,61	0,87				
R-235-2	1029,1	1091,68	1,06				
R-235-3	1176,9	1184,02	1,01				
R-235-4	1284,6	1302,09	1,01				
R-235-5	1287,6	1366,50	1,06	1,06	0,10	0,09	
R-345-1	1164,4	1314,59	1,13	1,00	0,10	0,09	
R-345-2	1414,6	1444,66	1,02				
R-345-3	1172,8	1392,87	1,19				
R-345-4	1456,7	1626,86	1,12				
R-345-5	1431,1	1689,95	1,18				

Looking at the tables above the finite element method showed that both geometric imperfections and residual stresses are essential for accurately predicting the ultimate strength of RHS columns. The removal of the residual stress brought as expected an overestimation of strength, highlighting its weaking effect. Meanwhile, eliminating the local imperfections resulted in an increase of the ultimate load as well, showing that local buckling was the dominant failure mode, considering that the removal of the global imperfections had a smaller effect of the outcome.

3.5.2 FE results from Shen & Wadee (2019a)

The FE model build from Shen & Wadee (2019a) uses the same geometric and material properties described earlier, more specifically two specimens have been selected, R-235-2 and R-345-1. The appropriate geometric properties, geometric imperfection and material properties of these specimens are listed in the tables below.

Table 7 Geometric properties and geometric imperfection sizes from Shen & Wadee (2019a)

Specimen	B/mm	D/mm	t/mm	L/mm	Local imperfection	Global imperfection
R-235-2	160,7	310,8	5,45	2780,4	d/294	L/1587
R-345-1	131,2	251,7	5,81	2250	d/209	L/877

Table 8 Material properties from Shen & Wadee (2019a)

Specimen	E/MPa	f _y /MPa	$\mathcal{E}_{\mathcal{Y}}$	\mathcal{E}_{St}	f_{u}/MPa	ε_u
R-235-2	2,07E+05	315,3	0,00152	0,0265	462,48	0,21
R-345-1	2,03E+05	416,25	0,00205	0,0145	575,91	0,132

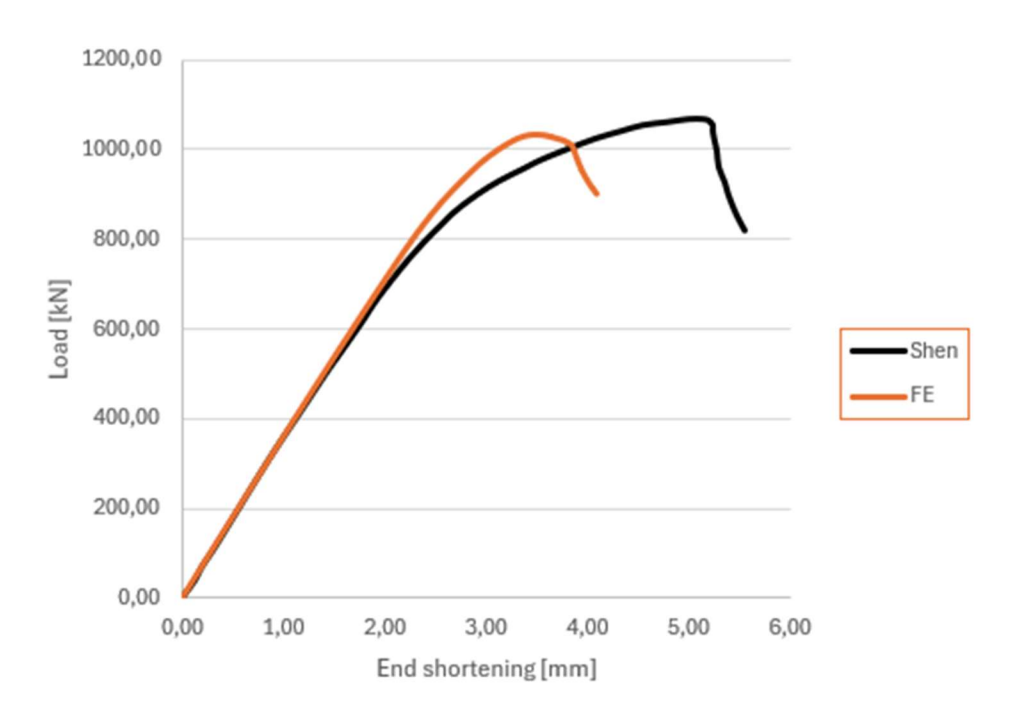


Figure 11 FE model and Shen's model longitudinal displacement comparison (R-235-2)

To continue with the validation of the accuracy from the FE model, the longitudinal displacement was plotted against the results published by Shen & Wadee (2019a) for the specimen R-235-2, were used for comparison. As shown in the figure above, the initial linear phase demonstrates an

ideal match, with both models capturing the elastic behavior consistently. Both curves reach comparable peak loads, although a slight change occurs in displacement behavior, the overall trend remains coherent. Most importantly, the ultimate load predicted by the FE model falls within the acceptable error range when compared to Shen's results. The minor differences are likely due to slight variations of the implemented boundary conditions, material properties or imperfection calibration.

Proceeding with the same strategy as before, to fully understand the behavior of RHS columns under axial load, it is necessary to perform multiple comparisons: the full model including geometric imperfections and residual stresses (case 1), the model without residual stresses (case 2), the model without local imperfections (case 3) and the model without global imperfections (case 4). Finally, for each case, it is compared to the ultimate load captured by the FE model with the experimental result.

Table 9 Ultimate load from Shen and FE model (case 1)

ALL

Specimen	Pult, Shen / kN	Pult, FE / kN	FE/Shen	Mean	SD	COV
R-235-2	1068,91	1028,92	0,96	0,97	0,01	0,01
R-345-1	1192,73	1162,22	0,97	0,97	0,01	0,01

Table 10 Ultimate load from Shen and FE model (case 2)

No Residual Stress

Specimen	Pult, Shen / kN	Pult, FE / kN	FE/Shen	Mean	SD	COV
R-235-2	1068,91	1254,54	1,17	1,19	0,03	0,02
R-345-1	1192,73	1442,19	1,21	1,19	0,03	0,02

Table 11 Ultimate load from Shen and FE model (case 3)

No Local Imperfections

Specimen	Pult, Shen / kN	Pult, FE / kN	FE/Shen	Mean	SD	COV
R-235-2	1068,91	1194,61	1,12	1 12	0,02	0,02
R-345-1	1192,73	1362,37	1,14	1,13		

Table 12 Ultimate load from Shen and FE model (case 4)

No Global Imperfections

Specimen	Pult, Shen / kN	Pult, FE / kN	FE/Shen	Mean	SD	COV
R-235-2	1068,91	1102,22	1,03	1,06	0.05	0.04
R-345-1	1192,73	1309,97	1,10	1,00	0,05	0,04

Looking at the tables above the finite element method showed that both geometric imperfections and residual stresses are essential for accurately predicting the ultimate strength of RHS columns. The removal of the residual stress brought as expected an overestimation of strength, highlighting its weaking effect. Meanwhile, eliminating the local imperfections resulted in an increase of the ultimate load as well, showing that local buckling was the dominant failure mode, considering that the removal of the global imperfections had a smaller effect of the outcome.

3.6 Automatization of the GMNIA

3.6.1 Automatization overview

Now that the created FE model is correct, some adjustments have been made before proceeding with further analyses by applying automated modeling and analysis.

Firstly, to simplify the modelling process and reduce computational load, <u>a quarter-symmetry representation</u> is considered. By applying symmetrical boundary conditions to all the relevant edges, it ensures coherence with the full structural behavior.

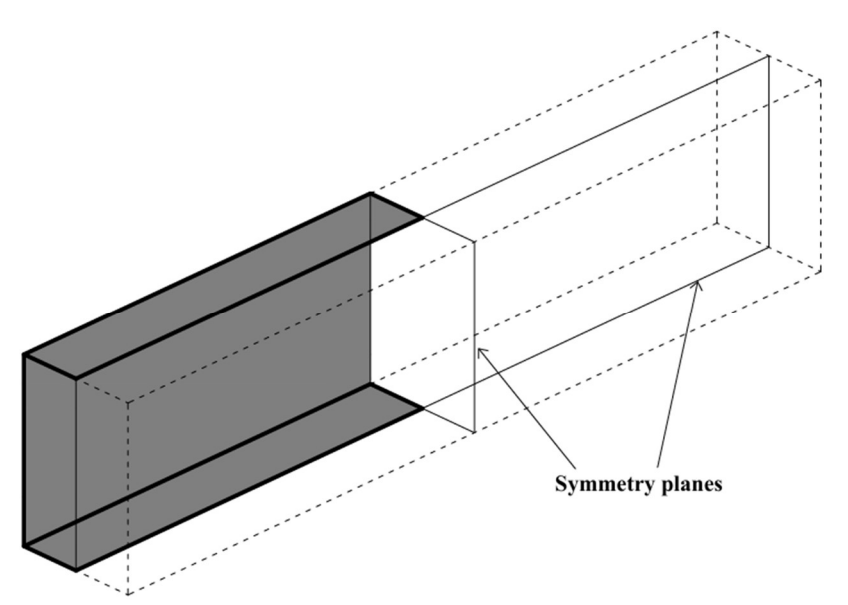


Figure 12 FE model symmetry simplification

Secondly, a strategic mesh refinement has been applied. Larger mesh size in both ends has been selected since those don't represent critical regions, while finer meshing is maintained in the critical regions to ensure accurate buckling results.

These modifications ensure that increasing efficiency, the accuracy of the model does not get lost, giving us the opportunity to achieve the required results.

3.5.1 Automated GMNIA's algorithm

Since we are developing a large database for rectangular hollow section steel columns which have various conditions, such as different cross-sectional parameters and slenderness ratio, a Python-based strategy can be established for automated processing. This would enable the conduction of the complete workflow in ABAQUS, including model generation, analysis execution and data extraction.

Building on established methodologies of ABAQUS scripting and the use of *rpy* files exported by ABAQUS, the automation of the modelling and analysis cycles is granted by an appropriate algorithm. The algorithm's general approach follows a structured workflow.

Initially, geometric and material data are imported from an external spreadsheet by Python who utilizes this information to create the complete ABAQUS model, according to the modeling details described in Chapter 3. Afterwards, a Linear Buckling Analysis (LBA) is conducted to determine the critical local and global buckling modes. To assign the initial geometric imperfection shapes to the GMNIA model, the lowest eigenvalues from local and global buckling modes are selected.

Following this, the model is then created, with the same process as outlined previously, with the appropriate material properties, the boundary conditions on each end and the Riks arc-length method is applied with displacement control to conduct the GMNIA process. Before running the simulation for the GMNIA analysis, the last modification required is to insert into the model the residual stresses due to welding conditions, which is done by modifying again the Python script.

In conclusion, the Python script provides the peak load, end-point displacement, end-point rotation and mid-span lateral displacement for every run for a single model and writes them in a spreadsheet as an output. This automated analysis establishes systematic investigation of the structural behavior of rectangular thin-walled columns under axial compression and supports further analysis under realistic conditions.

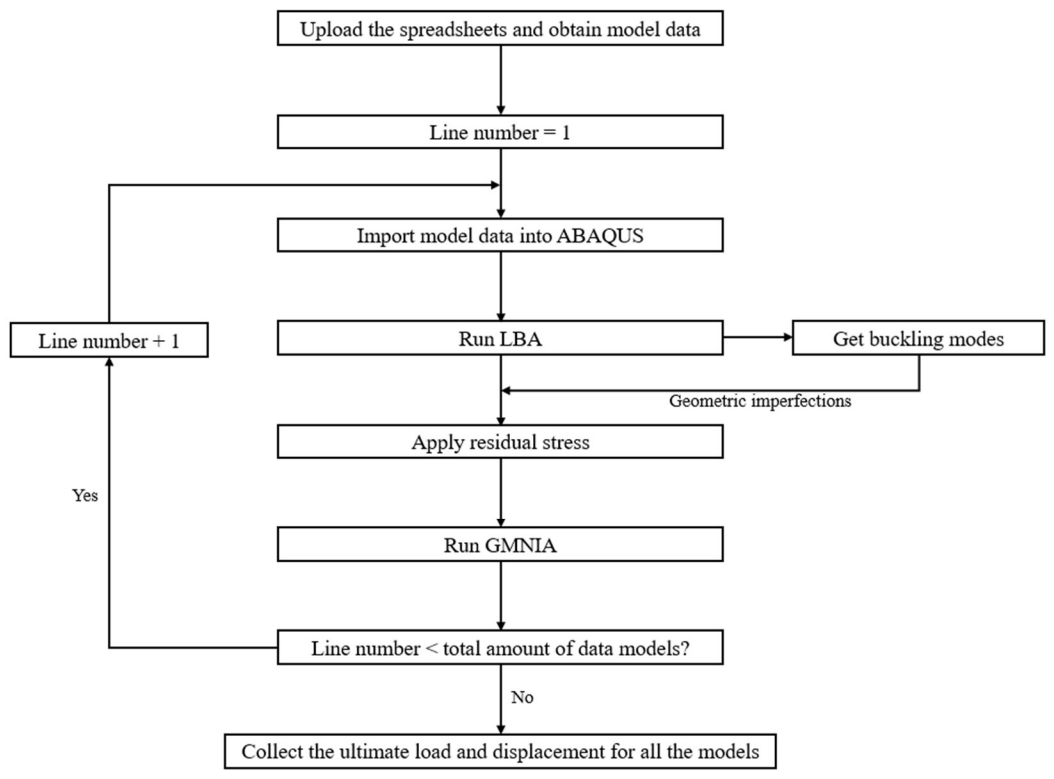


Figure 13 GMNIA automated process

4. Design standards and preliminary analysis

4.1 EC3 design guidance

4.1.1 Flexural buckling design in EC3 (2005)

The first step of designing the flexural buckling of a member requires the classification of the cross-section into one of four categories: Class one to Class four. This classification depends on the width-to-thickness ratio of the elements and the limit strain ε , which is calculated as:

$$\varepsilon = \sqrt{\frac{235}{f_y}}$$
 with f_y in N/mm² (4.1)

For members in compression, a Class 3 section must satisfy the following criteria:

$$\frac{c}{t} \le 42\varepsilon \tag{4.2}$$

Where c denotes the width of the area in compression and t is the thickness of the element.

According to BS EN 1993-1-1 (2005), for Class 1 to Class 3 sections of columns with thick sections, only flexural buckling needs to be considered. The design ultimate load is obtained using for following formula:

$$N_{b,Rd} = \frac{\chi A f_y}{\gamma_{M1}} \tag{4.3}$$

Where χ is the reduction factor derived from the Perry-Robertson formulation, A is the gross area, f_y is the yield strength and γ_{M1} is the partial factor for buckling (typically 1.0).

The reduction factor χ is obtained as:

$$\chi = \frac{1}{\phi + \sqrt{\phi^2 - \overline{\lambda}^2}} , \ \chi \le 1.0 \tag{4.4}$$

$$\phi = 0.5[1 + \alpha(\bar{\lambda} - 0.2) + \bar{\lambda}^2] \tag{4.5}$$

$$\bar{\lambda} = \sqrt{\frac{Af_y}{N_{cr}}} \tag{4.6}$$

Where the α is the imperfection factor and $\bar{\lambda}$ is the non-dimensional slenderness. The initial imperfection factor can be denoted as η_{EC3} :

$$\eta_{EC3} = \alpha (\bar{\lambda} - 0.2) \tag{4.7}$$

The elastic critical load N_{cr}, for the buckling mode is given by:

$$N_{cr} = \frac{\pi^2 EI}{(kL)^2} \tag{4.8}$$

Where I is the cross-section's minimum second moment of area about the axis of buckling, E is the Young's modulus, L is the length and k is the effective length factor depending on the boundary conditions (typically for simply-supported conditions k=1).

Meanwhile, for Class 4 sections, the gross area A is replaced by the effective area A_{eff}, leading to:

$$N_{b,Rd} = \frac{\chi A_{eff} f_y}{\gamma_{M1}} \tag{4.9}$$

$$\bar{\lambda} = \sqrt{\frac{A_{eff}f_y}{N_{cr}}} \tag{4.10}$$

4.1.2 Local buckling design in EC3 (2006)

Differently from global buckling, local buckling is usually analyzed for each plate individually. In BS EN 1993-1-5 (2006) it has been introduced the use of the effective cross-sectional area to capture the influence of local buckling. The ultimate load for local buckling is:

$$N_{c,Rd} = \frac{A_{eff}f_y}{\gamma_{M0}} \tag{4.11}$$

Where γ_{M0} is the partial factor for yielding (typically is taken 1.0), f_y is the yield stress of the material and A_{eff} is the effective area computed as the sum of the effective areas of each plate of the cross-section.

$$A_{eff} = \sum A_{c,eff} = \sum \rho A_c \tag{4.12}$$

Where A_c is the gross cross-sectional area of the plate. ρ is the reduction factor due to local buckling and it is calculated as:

$$\rho = \frac{\overline{\lambda}_p - 0.22}{\overline{\lambda}_p^2} \le 1 \tag{4.13}$$

With $\bar{\lambda}_p$ being the plate slenderness:

$$\bar{\lambda}_p = \sqrt{\frac{f_y}{\sigma_{cr}}} \tag{4.14}$$

And the critical stress for local buckling σ_{cr} is:

$$\sigma_{cr} = \frac{k_p \pi^2 E}{12(1 - v^2) \left(\frac{b}{t}\right)^2} \tag{4.15}$$

 k_p represents the buckling coefficient, typically taken as 4.0 for plates under uniform compression. b is the width of the plate, t is the thickness of the plate, E is the Young's modulus and ν is the Poisson's ratio.

4.1.3 Interaction between global and local buckling in EC3 (2005)

According to EC3 (2005), Class 4 sections have the highest width-to-thickness ratio. For these types of sections, members who go under compression might be faced with buckling interaction, where both global and local buckling can occur simultaneously. To take into account this interaction, EC3 merges together the effective area and the reduction factor, as shown in the next equation:

$$N_{b,Rd} = \frac{\chi A_{eff} f_y}{\gamma_{M1}} \tag{4.16}$$

Where f_y is the yield stress of the material, χ is the reduction factor for buckling, γ_{M1} is the partial factor for the instability resistance (typically is taken 1.0) and A_{eff} is the effective area of the cross-section, containing the effective area of each plate (top flange, bottom flange and the two webs).

Combining global and local buckling, EC3 predicts the ultimate load of a member under buckling. While being conservative in some scenarios, this approach used in recent studies has led to unsafe results due to the underestimation of the interactive effect.

Consequently, this project proposes to use finite element (FE) simulations and parametric studies to compare EC3 predictions against real world conditions for the ultimate load of compressed thinwalled rectangular hollow section steel columns.

4.2 FE model and EC3 design curve comparison

The comparison between the data simulated by the FE model and the theoretical results calculated in line with the EC3 provisions requires a broader range of initial conditions and geometric parameters to be covered by the FE model. The iterative analysis involves a square hollow section thin-walled steel column with S355 steel grade and ECCS distribution model for the residual stress. This part of the study consists of three data sets, with length and cross-sectional thickness that vary, since these are the primary parameters affecting the local and global buckling of the column. The specific properties of the models are shown in the table below.

Set 1 Set 2 Set 3 150mm x 150mm Cross-section Thickness t [mm] 5 3 4 Length L [mm] 1000 - 12000 0,22 - 2,65Global slenderness $\bar{\lambda}$ 0,19 - 2,250,21 - 2,50Plate slenderness $\bar{\lambda}_n$ 0.65 1,08 0.81

Table 13 FE model range of geometric properties

With the various geometric properties of the members, the ultimate load for each case can be established. To have a deeper insight into how to load-bearing capacity changes with the slenderness and more specifically how buckling interaction changes as both global and local slenderness changes, it is necessary to process the simulation data.

To isolate the influence of global slenderness, all the data that have the same plate slenderness are grouped separately, which corresponds to each set (Set 1 to Set 3). This allows us to have a clear observation on how the buckling interaction varies with the varying of the global slenderness when the cross-sectional properties remain unchanged. Then , the ultimate load, extracted from all the data, is normalized to obtain the reduction factor χ according to EC3 (2005), defined as below.

$$\chi = \frac{N_{b,Rd} \gamma_{M1}}{A_{eff} f_y} \tag{4.17}$$

With this approach, the relationship between the reduction factor χ and the global slenderness $\bar{\lambda}$, resulting from the changes of the geometric properties according to each group, can be established as illustrated below.

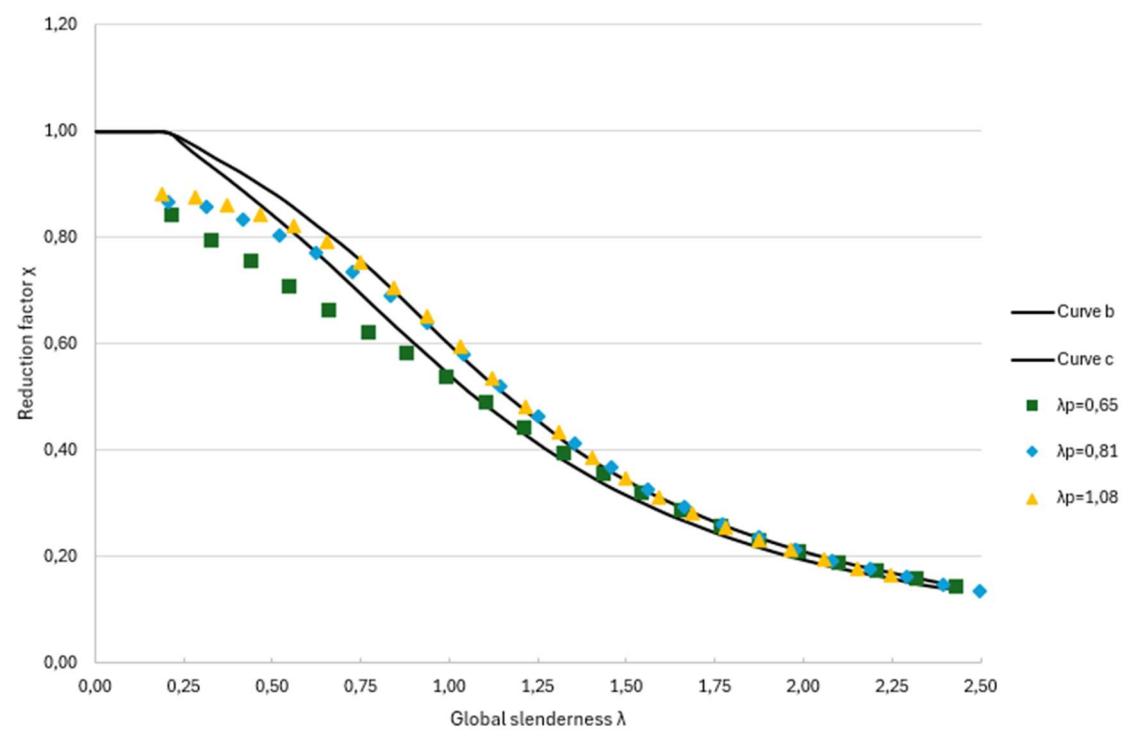


Figure 14 FE model curve and EC3 curve comparison

According to the graph above, an increase in the global slenderness $\bar{\lambda}$ shows a reduction in the load-bearing capacity for each case of plate slenderness $\bar{\lambda}_p$. The decreasing trend of the actual behavior driven by interactive buckling and residual stresses can be noticed to be very similar to the trend predicted from the EC3 (2005). Nevertheless, for low values of global slenderness, the normalized reduction factor χ falls below the EC3 prediction. As global slenderness increases, the FE results gradually converge toward the EC3 buckling curves. These discrepancies indicate that EC3 may overestimate or underestimate the ultimate load capacity in the presence of the interactive buckling and residual stresses, leading to the limitation of the effective width method (EWM) itself.

Meng et al. (2024) likewise demonstrated the inaccuracy of the EWM to capture the behavior of the local and global buckling interaction due to its simplified assumptions about cross-sectional effectiveness. To correct this, the results obtained by the FE models were reprocessed using a different approach to normalization. While the effective area and yielding stress can be unreliable in the denominator of the reduction factor formula, it was replaced with the ultimate load of the stub column obtained directly from FE simulations ($N_{eff,FE}$). The length of each stub column was set to three times the cross-section's width, ensuring that the response was governed by only local buckling.

$$\chi = \frac{N_{b,Rd} \gamma_{M1}}{N_{eff,FE}} \tag{4.18}$$

This adjustment eliminates the inaccuracies resulting from the EWM and provides a more physically meaningful comparison with EC3. The adjusted results are illustrated below.

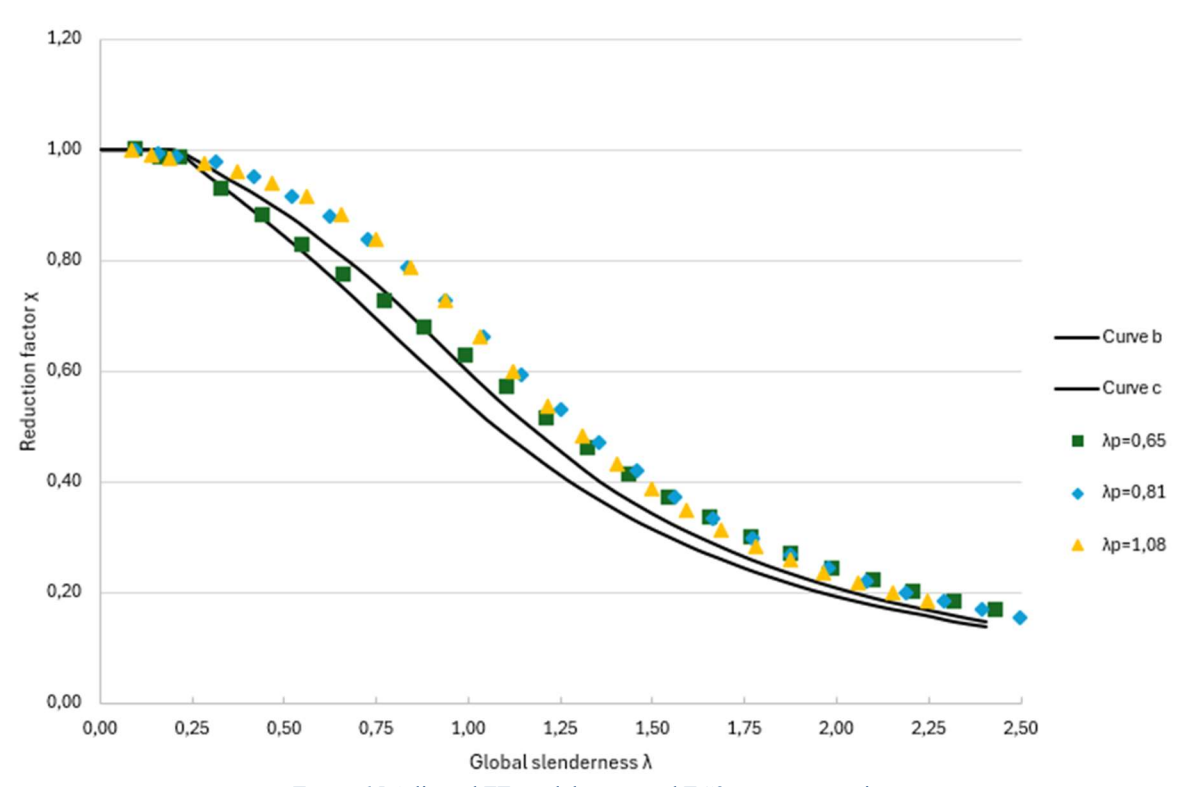


Figure 15 Adjusted FE model curve and EC3 curve comparison

As shown in the figure above, even with the removal of the inaccuracies from the EWM design approach, there are still present differences across the actual capacity of the columns and the EC3 predictions. The discrepancies for low values of global slenderness ($\bar{\lambda} < 0.2$) observed before in Fig. 15 are significantly reduced. As it can be seen in most cases when compared to the different plate slenderness trend, the EC3 design curve tends to have overconservative predictions. Nevertheless, in the case when the plate slenderness is 0.65 and the global slenderness falls between 0.2 and 1, the EC3 design curves tends to have unconservative predictions, since the actual ultimate load falls below the design curves provided by EC3.

These differences between FE model data and EC3 design curve may bring risk for the design of these structural elements and it is required to understand the reasons. One of the primary factors that can influence these deviations from the EC3 design curve is the imperfection sensitivity. The imperfection sensitivity means that the presence of even small imperfections along the element can cause buckling and a decrease in the theoretical critical load. Meng et al. (2024) study also showed that the ultimate strength remains affected by imperfections, especially in the local—global interaction range. According to their conclusion, it can be established that the imperfection sensitivity can vary depending on the interaction between local and global buckling modes.

Furthermore, the influence of the residual stresses on the ultimate capacity of the structural element and stiffness degradation is consistent with the findings of Shen & Wadee (2019a). The presence of residual stress was found to weaken the ultimate capacity compared to the models that were not subjected to residual stress. Considering that independently of the plate slenderness the trend does not change, enforcing again the FE's models ultimate load buckling curve remains uninfluenced by the imperfection sensitivity.

5. Parametric study

A parametric study was held to better investigate the complex behavior of thin-walled steel struts by using finite element (FE) models, S355 steel grade and ECCS distribution model for the residual stress. The struts used are rectangular hollow sections (RHS) with varying width and length in order to capture a wider range of both global slenderness $\bar{\lambda}$ and plate slenderness $\bar{\lambda}_p$. As discussed in the previous chapter, the reduction factor χ was calculated by normalizing the ultimate load obtained from the FE models against the ultimate load of the stub column obtained from FE simulations as well.

Cross-section	100mm x 100mm - 280mm x 280mm
Thickness t [mm]	3
Length L [mm]	300 - 30500

0,72 - 2,02

Table 14 Geometric properties for parametric study

In order to understand how the definition of the global slenderness $\bar{\lambda}$ affects the interpretation of the results, two types of global slenderness were considered: one based on the effective cross-sectional area A_{eff} (consistent with EC3 design guidance) and another based on the gross area A. This approach brings a direct comparison on how these considerations influence the buckling response.

5.1 Global slenderness using A_{eff}

T

5.1.1 Reduction factor vs Global slenderness

Plate slenderness

When the global slenderness $\bar{\lambda}$ is computed using the effective cross-sectional area, the results align closely with the assumption of the EC3 buckling curves. As shown in the figure below, the reduction factor χ decreases with increasing the global slenderness $\bar{\lambda}$ following the general trend of the EC3 buckling curves.

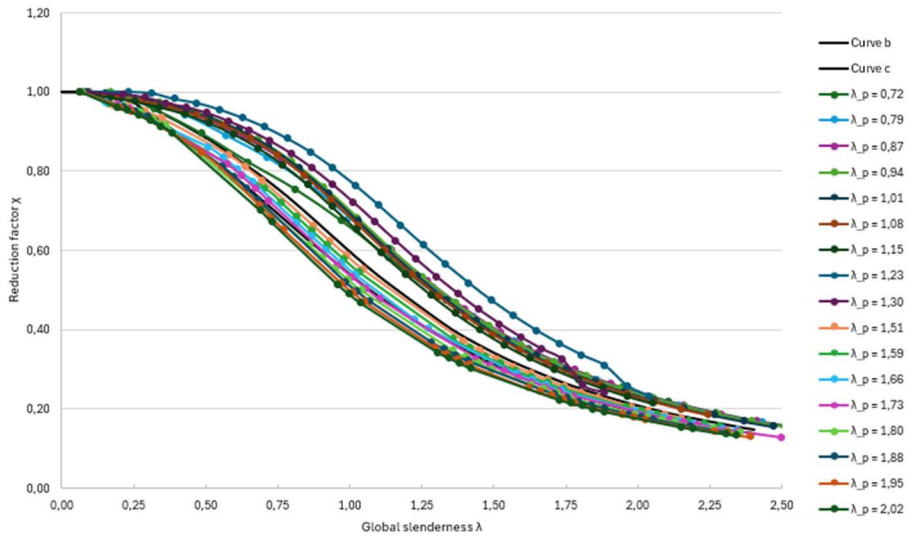


Figure 16 Reduction factor χ vs global slenderness $\bar{\lambda}$ calculated using the effective area

With plate slenderness $\overline{\lambda_p}$ increasing, the calculated buckling curves tend to shift downward. Two distinct cases can be observed: for lower values of plate slenderness (approximately $0.72 \le \overline{\lambda_p} \le 1.30$), the calculated reduction factor χ indicates an overestimation of capacity. On the other hand, for higher values of plate slenderness (approximately $1.51 \le \overline{\lambda_p} \le 2.02$), the reduction factor χ falls below the EC3 curves, indicating a conservative prediction.

This downward shift of the calculated curves approves that thin-walled members are increasingly susceptible to local buckling. The greater the plate slenderness $\overline{\lambda_p}$ the lower the effective stiffness, and the more severe is the strength capacity captured by the FE simulations.

To better examine how interaction evolves, specific values of global slenderness $\bar{\lambda}$ were considered: approximately 1.0, 1.75 and 2.0. The figure below displays the variation of the reduction factor χ against the plate slenderness $\bar{\lambda}_p$ for each case. The results were interpreted through the Van der Neut (1969) model, where the structural response is classified into different zones based on the interaction between local and global buckling and on the presence of material plasticity.

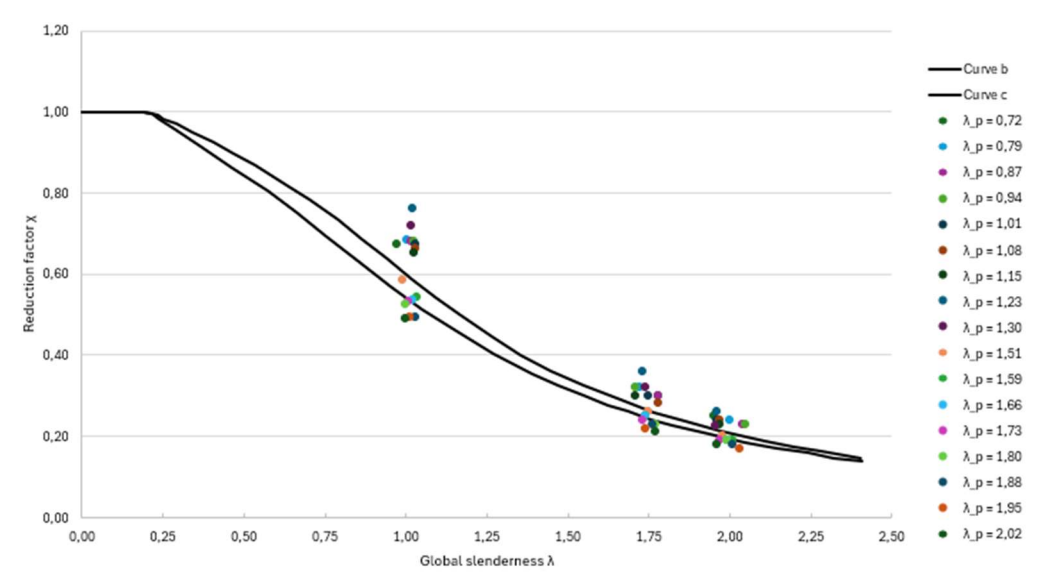


Figure 17 Reduction factor χ vs plate slenderness $\overline{\lambda}_p$ for fixed global slenderness $\bar{\lambda}$

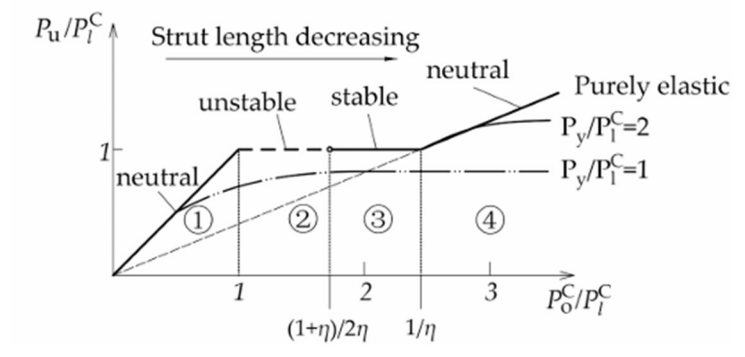


Figure 18 Van der Neut's curve model

Table 15 Summary of plate slenderness $\overline{\lambda}_p$, global slenderness $\overline{\lambda}$, reduction factors χ , and local-global buckling ratios

$\overline{\lambda_p}$	$\bar{\lambda}$	χ	$N_{cr,loc}$ / $N_{cr,gl}$	$\bar{\lambda}$	χ	$N_{cr,loc}/N_{cr,gl}$	$\bar{\lambda}$	χ	$N_{cr,loc}$ / $N_{cr,gl}$
0,72	0,97	0,67	1,82	1,78	0,3	6,12	1,95	0,25	7,28
0,79	1,00	0,68	1,59	1,72	0,32	4,68	2	0,24	6,37
0,87	1,02	0,68	1,38	1,78	0,3	4,23	2,04	0,23	5,53
0,94	1,03	0,68	1,20	1,71	0,32	3,33	2,05	0,23	4,79
1,01	1,03	0,67	1,04	1,75	0,3	3,01	1,96	0,24	3,76
1,08	1,03	0,66	0,91	1,78	0,28	2,7	1,97	0,24	3,3
1,15	1,03	0,65	0,79	1,71	0,3	2,2	1,97	0,23	2,91
1,23	1,02	0,76	0,69	1,73	0,36	1,99	1,96	0,26	2,56
1,30	1,01	0,72	0,61	1,74	0,32	1,79	1,96	0,22	2,27
1,51	0,99	0,59	0,43	1,75	0,26	1,33	1,98	0,2	1,71
1,59	1,03	0,54	0,43	1,74	0,25	1,21	2,01	0,19	1,61
1,66	1,02	0,54	0,38	1,74	0,25	1,1	1,99	0,19	1,44
1,73	1,01	0,53	0,34	1,73	0,24	1	1,97	0,19	1,30
1,80	1,00	0,52	0,31	1,77	0,23	0,96	1,99	0,19	1,22
1,88	1,03	0,49	0,30	1,76	0,23	0,88	2,01	0,18	1,15
1,95	1,01	0,49	0,27	1,74	0,22	0,8	2,03	0,17	1,08
2,02	1,00	0,49	0,25	1,77	0,21	0,77	1,96	0,18	0,94

For $\bar{\lambda} \approx 1.0$, the ratio $N_{cr,loc}$ / $N_{cr,gl}$ reaches values above and below one, indicating a shift from global buckling dominance to local-global buckling interaction as plate slenderness $\overline{\lambda_p}$ increases. This range falls into the transition between zone 1 and zone 2 in the Van der Neut curve, where the imperfection sensitivity is the highest, especially those who fall in zone 2 (Shen, 2018) . This is reflected also in the wide spread of the reduction factor χ , which decreases with $\overline{\lambda_p}$ increasing.

Meanwhile, as the strut length increases and the value of the global slenderness reaches $\bar{\lambda} \approx 1.75-2.0$, failure is governed by the elastic global buckling. This behavior corresponds to Van der Neut's zone 1, where the role of the plate slenderness becomes secondary. As $\bar{\lambda}_p$ increases, the N_{cr,loc} / N_{cr,gl} gradually approaches one, indicating the transition toward zone 2 where the local buckling starts contributing. The longer struts show more uniform behavior, with lower spread of the reduction factor γ .

5.1.2 Critical loads ratio vs Ultimate loads ratio

To investigate how the size of steel rectangular hollow section (RHS) members influences the interaction between local and global buckling, the results obtained from the FE models were compared against the EC3 predictions. The ratio N_{ult,FE}/N_{ult,EC3} was plotted against N_{cr,loc}/N_{cr,gl} to evaluate the extent of interaction between buckling modes. The EC3 ultimate load is calculated according to BS EN 1993-1-1:2005:

$$N_{ult,EC3} = \chi \frac{A_{eff} f_y}{\gamma_{M1}} \tag{5.1}$$

Where f_y is the yield stress of the material, χ is the reduction factor for buckling, γ_{M1} is the partial factor for the instability resistance (typically is taken 1.0) and A_{eff} is the effective area of the cross-section, containing the effective area of each plate (top flange, bottom flange and the two webs).

The reduction factor χ is found as:

$$\chi = \frac{1}{\phi + \sqrt{\phi^2 - \bar{\lambda}^2}} \le 1.0$$

$$\phi = 0.5 \left[1 + \alpha \left(\bar{\lambda} - 0.2 \right) + \bar{\lambda}^2 \right]$$

$$\bar{\lambda} = \sqrt{\frac{A_{eff} f_y}{N_{cr,gl}}}$$
(5.2)

Where α is an imperfection factor, which in this case is taken as 0.34 and $N_{cr,gl}$ is the global critical buckling load.

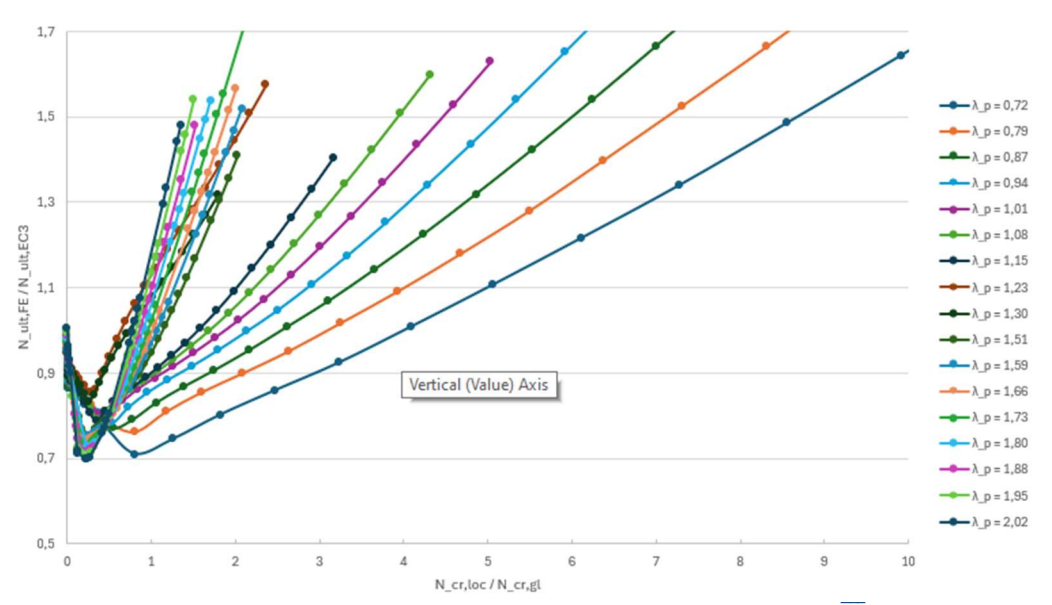


Figure 19 $N_{cr,loc}/N_{cr,gl}$ vs $N_{ult,FE}/N_{ult,EC3}$ for different plate slenderness $\overline{\lambda_p}$

The results from the figure above are displayed in the form of V-shaped curves and each curve corresponds to a different plate slenderness $\overline{\lambda_p}$. For smaller sections the interaction point points are closer to $N_{cr,loc}/N_{cr,gl}=1$, showing a balanced interaction between the two buckling modes. Increasing the cross-section size of the RHS, while maintaining the plate thickness constant, makes the member slenderer. This transforms the local buckling to the dominant mode, which is reflected by decreasing the values of $N_{cr,loc}/N_{cr,gl}$.

With the plate slenderness $\overline{\lambda_p}$ increasing, the minimum point of the curve, which represents the most severe capacity reduction due to combined buckling effects, tends to shift leftward. The left side of each curve corresponds to strongly dominant local buckling and the right side represents the configurations where the global buckling starts becoming more influential. The interaction between the local and global buckling modes is not perfectly symmetrical, emphasizing the effect of imperfection sensitivity when two buckling modes interact with thin-walled members.

The ratio N_{ult,FE}/N_{ult,EC3} can provide results on how conservative the EC3 predictions are. When local buckling is dominant, the curve shows values greater than 1, indicating that EC3 is more conservative. On the other hand, around the interaction region, the ratio falls below 1, meaning that EC3 overestimates the capacity of the members becoming non-conservative. As the global buckling becomes more dominant, EC3 regains conservatives. This behavior reflects once again the limitations of EC3 in accounting for interactive buckling within RHS members.

5.2 Global slenderness using gross area A

5.2.1 Reduction factor vs Global slenderness

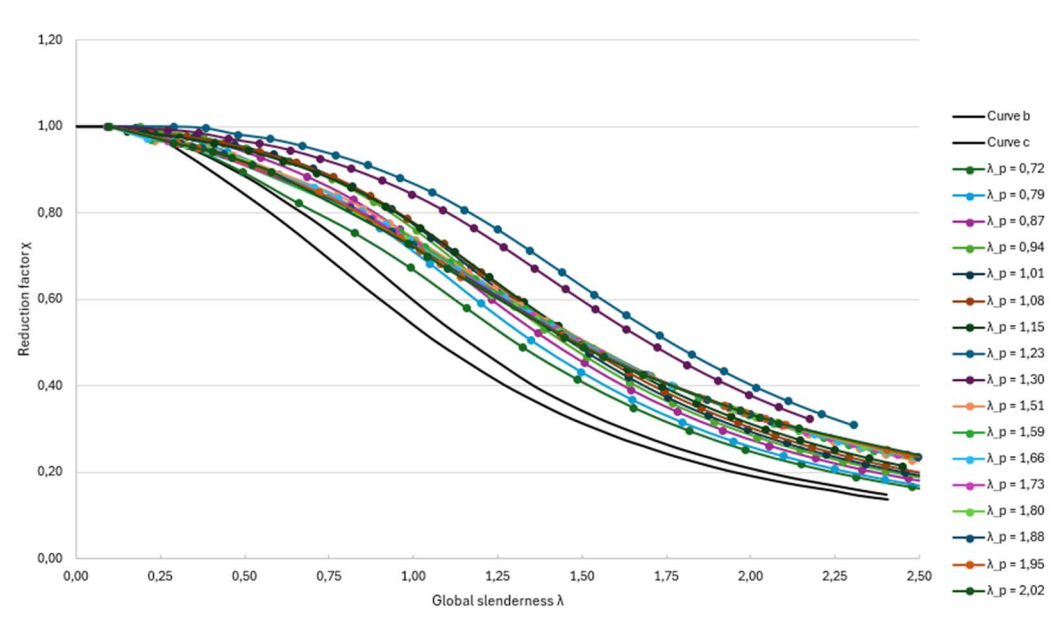


Figure 20 Reduction factor γ vs global slenderness $\bar{\lambda}$ calculated using the gross area

When the global slenderness $\bar{\lambda}$ is calculated using the gross area A of the cross-section, the same reduction factor χ appears at higher slenderness values as shown in the figure above. This occurs because considering the gross area, the stiffness of the members is greater than it actually is, increasing the value of slenderness:

$$\bar{\lambda} \propto \sqrt{A} = A_{gross} > A_{eff} = \bar{\lambda}_{gross} > \bar{\lambda}_{eff}$$
 (5.3)

The calculated FE ultimate loads remain unchanged, meaning that when they are plotted against higher of slenderness the curves shift rightward and they appear above the EC3 buckling curves. This shift gives the impression that each model outperforms the design curves. For this reason, the appropriate area must be used to avoid misinterpretation of the capacity.

The effect of increasing plate slenderness $\overline{\lambda_p}$ it is easily visible even in this case. As $\overline{\lambda_p}$ increase, the reduction factor χ decreases across the global slenderness range, confirming that local buckling reduces the overall strength of the member.

5.2.2 Critical loads ratio vs Ultimate loads ratio

To evaluate the influence of the assumptions for the area of the cross-section, gross area A is used in the computations of both global slenderness $\bar{\lambda}$ and the design ultimate load $N_{ult,EC3}$ according to EC3.

$$N_{ult,EC3,g} = \chi \frac{A f_y}{\gamma_{M1}} \tag{5.4}$$

The reduction factor χ is found as:

$$\chi = \frac{1}{\phi + \sqrt{\phi^2 - \bar{\lambda}^2}} \le 1.0$$

$$\phi = 0.5 \left[1 + \alpha \left(\bar{\lambda} - 0.2 \right) + \bar{\lambda}^2 \right]$$

$$\bar{\lambda} = \sqrt{\frac{A f_y}{N_{cr,gl}}}$$
(5.5)

Where α is an imperfection factor, which in this case is taken as 0.34 and $N_{cr,gl}$ is the global critical buckling load.

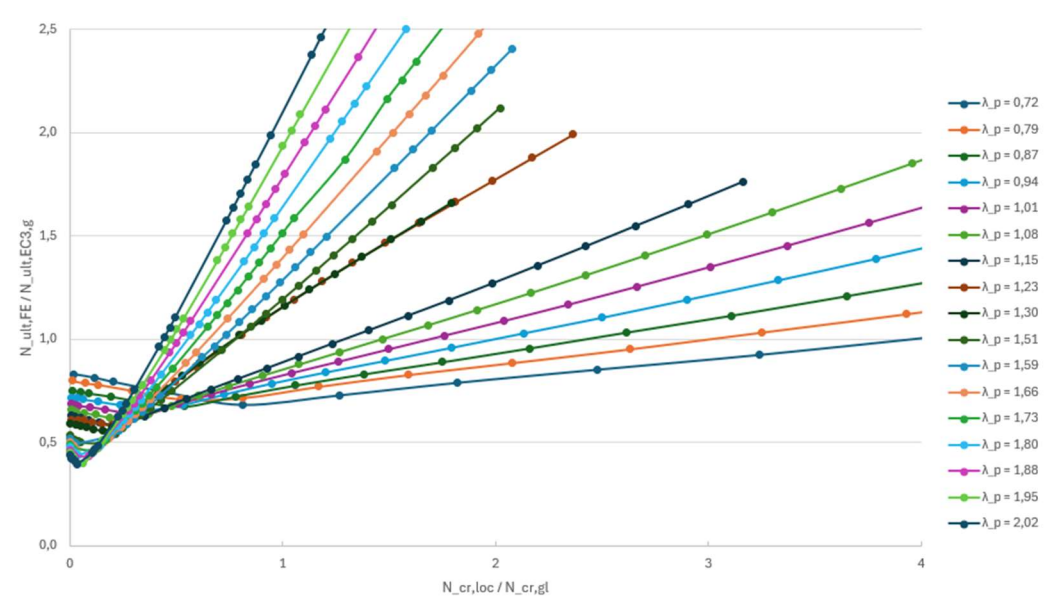


Figure 21 N_{cr,loc}/N_{cr,gl} vs N_{ult,FE}/N_{ult,EC3,g} for different plate slenderness $\overline{\lambda_p}$

The results from the figure above are still displayed in the shape of V-shaped curves, where each line represents a different plate slenderness $\overline{\lambda_p}$. The use of the gross area brings no reduction in capacity due to local instability. The smaller the sections the closer the minimum points are to $N_{cr,loc}/N_{cr,gl}=1$. With plate slenderness $\overline{\lambda_p}$ increasing, the minimum point of the curve, which represents the most severe reduction in capacity due to buckling interaction, shifts gradually to the left and downward. As in the previous case, the interaction between local and global critical loads is not symmetrical and the sensitivity to imperfections remains a key factor.

Using gross area A, the ratio $N_{ult,FE}/N_{ult,EC3,g}$ decreases significantly across all curves. Even when the local buckling is the dominant one, most values are below 1, meaning that EC3 overestimates the load capacity and it can be considered non-conservative. Only in the global buckling dominant part the use of gross area A remains conservative. This gives one more reason to use the effective cross-sectional area for thin-walled structures to ensure safe and realistic analysis.

6. Conclusions

This final year's project investigates the interactive buckling behavior of thin-walled rectangular steel section columns subjected to axial compression through a point load. Using advanced software to carry on with finite element analysis (FEA), like ABAQUS, it was able to accurately simulate the realistic effects of boundary conditions, geometric imperfections, residual stresses and nonlinearity of materials, which further helped the analysis of the interaction between local and global buckling modes. Experimental data from Yang et al. (2017) and numerical results from Shen & Wadee (2019a) were attested to confirm the adequate performance of the FE models in predicting both ultimate loads and failure modes.

To enable an extensive parametric investigation, the entire analysis process was automated by implementing Python scripting, which significantly enhanced its efficiency. The results showed that plate slenderness played a crucial role in determining the dominant failure mechanism since increasing the plate slenderness shifted the response toward local buckling behavior. On the other hand, including residual stresses caused a reduction in the ultimate load capacity, highlighting their detrimental effect when geometric imperfections are included as well.

When compared to EC3 design predictions, it was revealed that designs were in some cases conservative and in other cases non-conservative, especially when plate slenderness was high. For this final year's project there was no involvement with modification proposals to current design methods. Nevertheless, when the validated finite element (FE) modeling process is considered along with the provided dataset, a solid foundation for future studies is established. This project provides a practical help for future research on involvement of imperfection sensitivity and buckling interaction, contributing to potential improvements to existing design guidelines for thinwalled structural members.

From an application standpoint, industries like offshore energy or prefabricated modular construction would benefit the most from more accurate design methodologies. Since these elements have a wide range of applications and benefits, it means that the exploitation of the post-buckling strength of thin-walled members could enable lighter, more material-efficient and sustainable structures.

Furthermore, interactive buckling is not an isolated problem limited to rectangular hollow sections, but a phenomenon which is present within a wide range of steel profiles. Thus, studying these structures through finite element modeling and validating them against experimental data contributes to filling the gap difference between theoretical studies and practical applications.

7. Acknowledgments

I would like to express my deepest gratitude to my supervisors Prof. Ahmer Wadee and Dr. Xin Meng, who have helped me deliver this thesis. Without the expertise of Prof. Wadee on buckling analysis and his effort on making me understand or the constant help of Dr. Meng on even the smallest details to make my work progress efficiently, this project would have been far from possible.

I also want to thank Prof. Francesco Tondolo for accepting my invitation to be my supervisor representative from Politecnico di Torino.

I am grateful to Politecnico di Torino for providing me with the opportunity to be an exchange student in of the most prestigious universities in the world, Imperial College London. I have learned a lot from both universities and I have also built a lot in my knowledge about Civil Engineering.

I would like to thank from the bottom of my heart my friends and family for being with me in every step of the way. They have always been there for me whenever I needed them most, emotionally and physically. These past few years would have been really difficult were it not for their presence and support. I cannot put it into words to express how grateful I am for being surrounded by all these people and I wish the very best for them all.

Last but not least, I want to thank me. I want to thank me for not giving up. I want to thank me for dealing with many challenges in the most stubborn way. I want to thank me for keeping the positivity and being there for all, no matter what. This has been a good journey and yet more to come.

Ersid Alushi June 2025

8. References

A. van der Neut, The interaction of local buckling and column failure of thin-walled compression members, Proceedings of the 12th International Congress on Applied Mechanics, Springer, 1969, pp. 389–399

Bai, L. & Wadee, M. A. (2015) Imperfection sensitivity of thin-walled I-section struts susceptible to cellular buckling. *International Journal of Mechanical Sciences*. 104 162–173. 10.1016/j.ijmecsci.2015.10.010.

Behzadi-Sofiani, B., Gardner, L., Wadee, M. A., Dinis, P. B. & Camotim, D. (2021) Behaviour and design of fixed-ended steel equal-leg angle section columns. *Journal of Constructional Steel Research*. 182 106649. 10.1016/j.jcsr.2021.106649.

BS EN 1993-1-1:2005: Eurocode 3. Design of steel structures. General rules and rules for buildings. British Standards Institute.

BS EN 1993-1-5:2006: Eurocode 3. Design of steel structures. Plated structural elements. British Standards Institute.

Degée, H., Detzel, A. & Kuhlmann, U. (2008) Interaction of global and local buckling in welded RHS compression members. *Journal of Constructional Steel Research*. 64 (7), 755–765. 10.1016/j.jcsr.2008.01.032.

Kwon, Y. B. & Seo, E. G. (2013) Prediction of the compressive strength of welded RHS columns undergoing buckling interaction. *Thin-Walled Structures*. 68 141–155. 10.1016/j.tws.2013.03.009.

Meng, X. & Gardner, L. (2020) Behavior and Design of Normal- and High-Strength Steel SHS and RHS Columns. *Journal of Structural Engineering (New York, N.Y.)*. 146 (11), 10.1061/(ASCE)ST.1943-541X.0002728.

Meng, X. & Gardner, L. (2021) Testing, modelling and design of normal and high strength steel tubular beam-columns. *Journal of Constructional Steel Research*. 183 106735. 10.1016/j.jcsr.2021.106735.

Meng, X., Whitfield, S., Boudjabeur, S. & Gardner, L. (2024) Stability of hot-finished and cold-formed steel hollow section columns: A comparative study. *Structures*. 68 107192. 10.1016/j.istruc.2024.107192.

Pavlovčič, L., Froschmeier, B., Kuhlmann, U. & Beg, D. (2012) Finite element simulation of slender thin-walled box columns by implementing real initial conditions. *Advances in Engineering Software*. 44 (1), 63–74. 10.1016/j.advengsoft.2011.05.036.

Rozylo, P., Rogala, M. & Pasnik, J. (2023) Buckling Analysis of Thin-Walled Composite Structures with Rectangular Cross-Sections under Compressive Load. *Materials*. 16 (21), 6835. 10.3390/ma16216835.

- Shen, J. (2018) *Interactive Buckling in Thin-Walled Rectangular Hollow Section Struts*, Ph.D. thesis. Imperial College London.
- Shen, J. & Wadee, M. A. (2019a) Local–global mode interaction in thin-walled inelastic rectangular hollow section struts part 1: Nonlinear finite element analysis. *Thin-Walled Structures*. 145 106183. 10.1016/j.tws.2019.106183.
- Shen, J. & Wadee, M. A. (2019b) Local–global mode interaction in thin-walled inelastic rectangular hollow section struts part 2: Assessment of existing design guidance and new recommendations. *Thin-Walled Structures*. 145 106184. 10.1016/j.tws.2019.106184.
- W.T. Koiter (1945) Over de stabiliteit van het elastisch evenwicht (On the Stability of Elastic Equilibrium), (in Dutch). Thesis, Technische Hoge School Delft. H.J. Paris, Amsterdam, 1945 (English translation: (a) NASA TTF-10.833, 1967; a Technical report No. AFFDL-TR-70-25
- Yang, L., Shi, G., Zhao, M. & Zhou, W. (2017) Research on interactive buckling behavior of welded steel box-section columns. *Thin-Walled Structures*. 115 34–47. 10.1016/j.tws.2017.01.030.
- Yun, X. & Gardner, L. (2017) Stress-strain curves for hot-rolled steels. *Journal of Constructional Steel Research.* 133 36–46. 10.1016/j.jcsr.2017.01.024.